How to cite: *Angew. Chem. Int. Ed.* **2022,** *61,* e202210498
International Edition: doi.org/10.1002/anie.202210498
German Edition: doi.org/10.1002/ange.202210498

Chemoproteomics | Hot Paper

Chemoproteomics-Enabled Identification of 4-Oxo-β-Lactams as Inhibitors of Dipeptidyl Peptidases 8 and 9

Luís A. R. Carvalho[+], Breyan Ross[+], Lorenz Fehr[+], Oguz Bolgi, Svenja Wöhrle, Kenneth M. Lum, David Podlesainski, Andreia C. Vieira, Reiner Kiefersauer, Rita Félix, Tiago Rodrigues, Susana D. Lucas, Olaf Groß, Ruth Geiss-Friedlander, Benjamin F. Cravatt, Robert Huber, Markus Kaiser, and Rui Moreira**

Abstract: Dipeptidyl peptidases 8 and 9 (DPP8/9) have gathered interest as drug targets due to their important roles in biological processes like immunity and tumorigenesis. Elucidation of their distinct individual functions remains an ongoing task and could benefit from the availability of novel, chemically diverse and selective chemical tools. Here, we report the activity-based protein profiling (ABPP)-mediated discovery of 4-oxo-β-lactams as potent, non-substrate-like nanomolar DPP8/9 inhibitors. X-ray crystallographic structures revealed different ligand binding modes for DPP8 and DPP9, including an unprecedented targeting of an extended S2′ (eS2′) subsite in DPP8. Biological assays confirmed inhibition at both target and cellular levels. Altogether, our integrated chemical proteomics and structure-guided small molecule design approach led to novel DPP8/9 inhibitors with alternative molecular inhibition mechanisms, delivering the highest selectivity index reported to date.

Introduction

The dipeptidyl peptidases 8 and 9 (DPP8/9) are members of the serine hydrolase subfamily S9B that cleave N-terminal dipeptides preferentially after a proline residue from substrates.[1] Both enzymes were originally identified as homologues of DPP4, a protease that plays a prominent role in glucose homeostasis by controlling gastrointestinal incretin hormones. DPP4 is an important target for the development of type II diabetes chemotherapies with several inhibitors in clinical use today.[2] Whereas DPP4 is extracellular, DPP8/9 appear primarily intracellular and perform distinct, non-DPP4-related biological functions. They are particularly known for their key roles in the immune response, e.g., by controlling inflammasome and pyroptosis activation.[3] In addition, they have also been implicated in many other biological processes such as apoptosis, adipogenesis, spermatogenesis, cell cycle regulation or chemosensitisation of Leukemia cells to cytotoxic agents.[4]

The assignment of individual DPP8 or DPP9 functions is an ongoing challenge and active line of research. While DPP8 has emerged as a relevant target for multiple myeloma cancers, a role in cell proliferation, migration and

[*] Dr. L. A. R. Carvalho,[+] A. C. Vieira, R. Félix, Dr. T. Rodrigues, Dr. S. D. Lucas, Prof. Dr. R. Moreira
Department of Pharmaceutical Sciences and Medicines, Research Institute for Medicines (iMed.ULisboa), Faculdade de Farmácia, Universidade de Lisboa
Av. Prof. Gama Pinto, 1649-003 Lisboa (Portugal)
E-mail: rmoreira@ff.ulisboa.pt

Dr. B. Ross,[+] Prof. Dr. R. Huber
Max Planck Institut für Biochemie
82152 PlaneggMartinsried (Germany)

Dr. B. Ross,[+] Dr. R. Kiefersauer
Proteros Biostructures GmbH
82152 PlaneggMartinsried (Germany)

Dr. L. A. R. Carvalho,[+] Dr. K. M. Lum, Prof. Dr. B. F. Cravatt
Department of Chemistry,
The Scripps Research Institute
La Jolla, California 92037 (USA)

O. Bolgi, Dr. R. Geiss-Friedlander
Center of Biochemistry and Molecular Cell Research
Albert-Ludwigs-Universität, 79104 Freiburg (Germany)

L. Fehr,[+] D. Podlesainski, Prof. Dr. R. Huber, Prof. Dr. M. Kaiser
Fakultät für Biologie, Zentrum für Medizinische Biotechnologie,
Universität Duisburg-Essen
45117 Essen (Germany)
E-mail: markus.kaiser@uni-due.de

Prof. Dr. R. Huber
Fakultät für Chemie, Technische Universität München
85747 Garching (Germany)

S. Wöhrle, Prof. Dr. O. Groß
Institut für Neuropathologie, Universitätsklinikum Freiburg
79106 Freiburg (Germany)

Prof. Dr. O. Groß
Signalling Research Centres BIOSS and CIBSS, University of Freiburg
79104 Freiburg (Germany)

[+] These authors contributed equally to this work.

invasion of non-small cell lung cancer was attributed to DPP9.[5] Furthermore, DPP9 has been identified as rate-limiting for the proteolytic processing of proline-containing cytosolic peptides and to modulate the presentation of proline-containing peptides by the MHC class I system, to regulate B-cell receptor-mediated signaling and repair of DNA damage.[6] Recently, DPP9 was also linked to severe Covid-19 disease progression.[7] Overall, it is becoming obvious that DPP8/9 display not only redundant but also distinct biological functions. Accordingly, chemical inhibitors with differential DPP8/9 inhibitory properties may represent promising chemical tools and serve as a starting point for future DPP8/9 selective chemotherapy development.

DPP8 and DPP9 share an overall identity of 58 % and an identity of 92 % in their active site.[8] Their overall structure is highly similar to DPP4 as all three enzymes have a highly conserved C-terminal α/β globular domain, which encompasses the catalytic triad, and an N-terminal β-propeller domain, where most ligand-binding elements reside and most structural variations between DPP4 and DPP8/9 are located. The S1 subsite is conserved in all three enzymes, but the S2 subsite diverges significantly and is larger in DPP8/9. The few small differences in the active site of DPP8 and DPP9 have little impact in the overall structure and reactivity due to mostly conservative amino acid substitutions.[9] Unlike DPP4, DPP8 and DPP9 undergo a rearrangement of a region called the R-helix upon ligand binding, which participates in the shaping of the substrate binding site. A key difference between DPP8 and DPP9 seems to be a region contained in the R-segment, a solvent exposed loop containing two consecutive histidines in DPP9 and aspartic acid and tyrosine in the analogous DPP8 positions.

Due to this high structural similarity and the lack of crystallographic data, which was only recently disclosed, the elucidation of selective DPP8 or DPP9 inhibitors has remained a demanding task.[8b] Despite this, several active-site substrate-like DPP8/9 inhibitors accommodating the S2–S1 subsites have already been developed and are regularly applied in biochemical and biological assays. These include non-covalent, reversible inhibitors such as 1G244, a moderately selective DPP8-inhibitor (≈4-fold selectivity vs. DPP9, no DPP4 inhibition) with an isoindoline scaffold at the P1-position and a bulky difluoro-benzhydryl-piperazine moiety at the P2-position (Figure 1).[10] Systematic variation of 1G244 then led to the development of 1G244-12n with a ≈10-fold DPP8 over DPP9 selectivity.[11] The peptide SLRFLYEG represents another non-covalent DPP8/9 selective inhibitor; this compound binds also in a substrate-like fashion to the active site.[12] An example for a reversible covalent inhibitor is the frequently used DPP broadband inhibitor Val-boroPro (VbP), also known as Talabostat, inhibiting DPP4/8/9 at comparable levels.[13] Finally, irreversible covalent inhibitors are also known, such as a phosphonate-based isoindoline derivative (Lys-phospho-isoindoline) with pronounced DPP8 over DPP4 selectivity;[14] unfortunately, its selectivity vs. DPP9 has not yet been reported.

Although these studies demonstrated that proper targeting of DPP8/9's S2–S1 subsites may generate DPP8/9 vs. DPP4 selective inhibitors, the strong structural homologies in these regions of the proteins complicate a design of DPP8 vs DPP9 selective inhibitors.[9] Indeed, crystallographic and cryoEM studies on the binding modes of 1G244, VbP (both to DPP8/9) and SLRFLYEG (to DPP8) revealed a highly similar and induced fit binding mode that includes a structural ordering of the R-helix located near the β-propeller domain upon inhibitor binding.[4e,15]

Stepping up to the DPP8 vs. DPP9 selectivity challenge therefore requires the development of strategies for identifying inhibitors with alternative binding modes and inhibitory profiles. An approach to identify and characterize inhibitory profiles of chemical compounds is activity-based protein profiling (ABPP).[16] In ABPP, chemical probes known as activity-based probes (ABPs) are used to covalently label the active sites of enzymes and provide dynamic profiles of their activities in complex proteomes.[17] ABPs, consisting mainly of a covalently binding reactive group and a reporter tag, require a catalytically active enzyme and a non-occupied active site for target labelling. Their application allows monitoring of enzyme activity under various physiological conditions, including after preincubation with potential inhibitors targeting and occupying their active sites. This 'competitive ABPP' approach generates a rapid inhibitor screening on the proteome level and provides early data on potency and selectivity.[16,18]

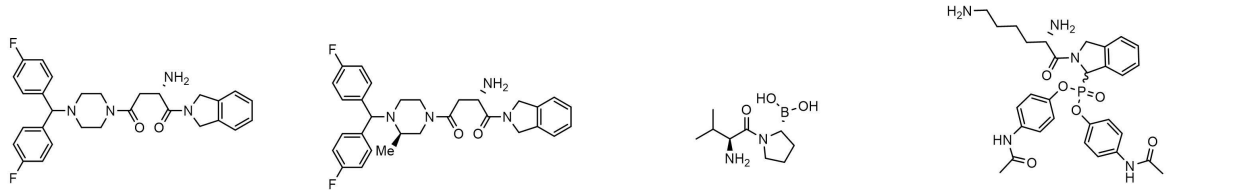

1G244, IC_{50} [nM]
DPP8: 14
DPP9: 53
DPP4: > 100'000

1G244-12n, IC_{50} [nM]
DPP8: 55
DPP9: 540
DPP4: > 50'000

VbP, IC_{50} [nM]
DPP8: 4
DPP9: 11
DPP4: < 4

Lys-phospho-isoindoline, IC_{50} [nM]
DPP8: 530
DPP9: N/A
DPP4: > 500'000

Figure 1. The development of DPP8/9-selective inhibitors remains a challenge. Chemical structures and inhibition potencies of selected DPP inhibitors; all known inhibitors target the S2–S1 subsites.

In the present study, we investigated the target repertoire of *N*-phenyl 4-oxo-β-lactams. These compounds are known to inhibit serine proteases such as human neutrophil elastase by a covalent binding mechanism, but their proteome-wide target engagement has remained unexplored.[19] We therefore performed ABPP experiments and serendipitously discovered that *N*-aryl-*meta*-substituted analogues are potent DPP8/9 inhibitors. Subsequent structure–activity-relationship studies and crystallographic analyses of their binding modes then revealed that DPP8 inhibition was based on a unique, non-substrate-like binding mode, which resulted in the best DPP8/9 selectivity index reported to date.

Results and Discussion

We first used a rhodamine-tagged 4-oxo-β-lactam ABP **1** in a gel-based ABPP approach to profile HEK293T and U937 whole cell lysates (Figure 2A, B).[20] Concentration-dependent labelling of distinct proteins was observed; at low and thus biologically more relevant concentrations (0.1–10 μM), only selected proteins, e.g. at a molecular weight of approximately 25, 75 and 100 kDa, were predominantly labelled, suggesting a distinct target selectivity which may open possibilities for the development of selective inhibitors.

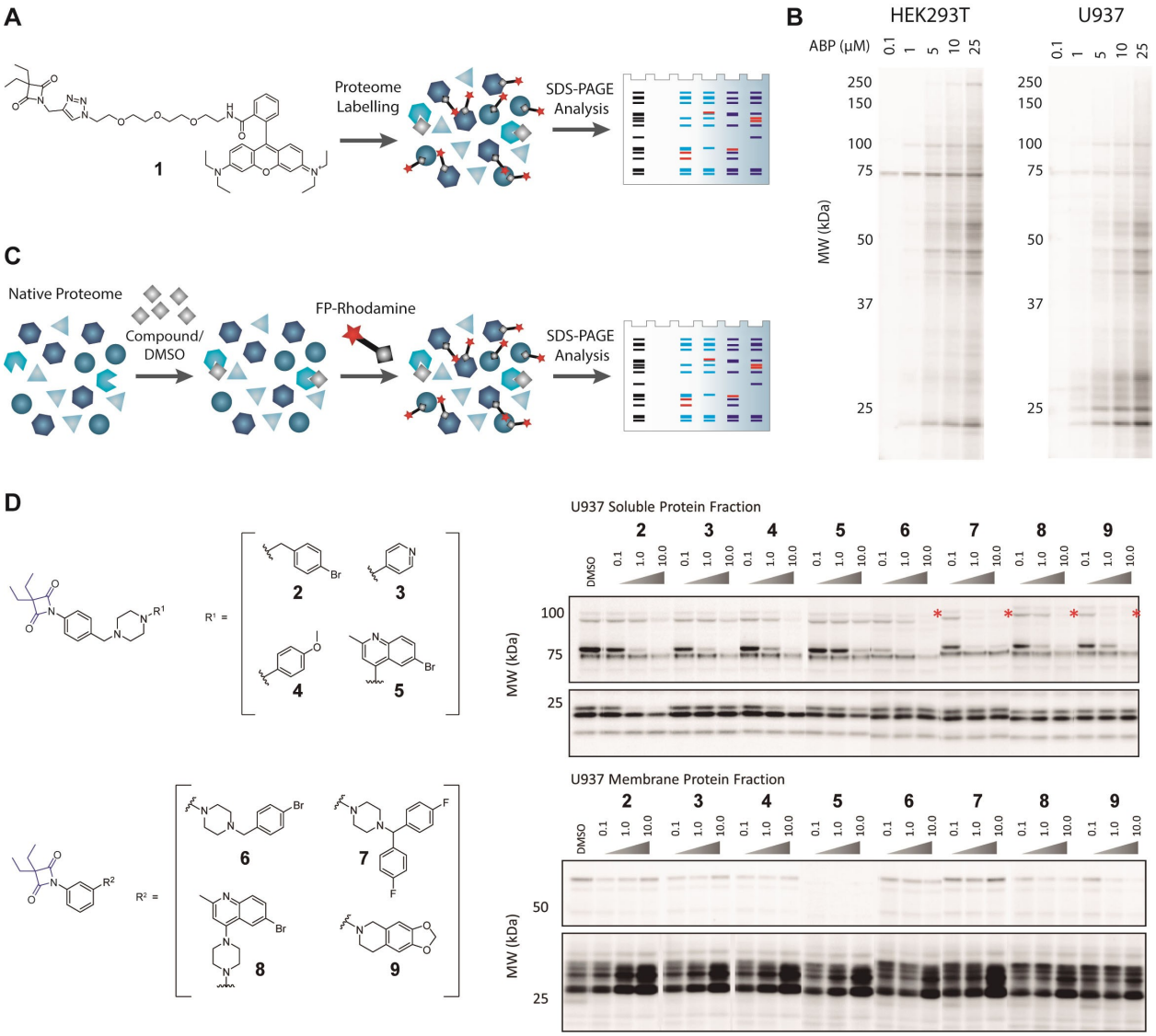

Figure 2. Reactivity analysis of the 4-oxo-β-lactam moiety using gel-based ABPP. A) The rhodamine-tagged 4-oxo-β-lactam ABP **1** was used in a comparative ABPP approach. B) Gel-based ABPP analysis of HEK293T and U937 whole cell lysates with different concentrations of ABP **1** revealed distinct and selective protein labelling. C) General competitive ABPP platform for competitive profiling of serine hydrolases. Native proteomes are treated with either a DMSO control or 4-oxo-β-lactams **2**–**9**, followed by general serine hydrolase labelling with the ABP FP-Rhodamine. Suppression of FP-Rhodamine labelling then indicates binding of 4-oxo-β-lactams to the active sites of serine hydrolases. D) Gel-based analysis of the competitive ABPP experiment of 4-oxo-β-lactams **2**–**9** in U937 whole cell lysates. Suppression of fluorescent signals at ca. 100 kDa in the soluble fraction (asterisks) suggest compound-mediated inhibition of DPP8/9.

To investigate if suitable modification of the 4-oxo-β-lactam reactive group would result in more selective compounds, a competitive ABPP approach with a focused library of *N*-phenyl 4-oxo-β-lactams with chemically diverse substitutions at the *para*-, *meta*- and *ortho*-position was next performed (Figure 2C, D). Fractioned U937 cell lysates were preincubated with varying concentrations of these 4-oxo-β-lactams, followed by general serine hydrolase labelling with the ABP fluorophosphonate-rhodamine (FP-Rh).[21] In this experimental setting, concentration-dependent disappearance of bands can be directly related to 4-oxo-β-lactam-triggered serine hydrolase inhibition. In contrast to compounds **2**–**5**, their *meta*-substituted counterparts **6**–**9** reduced FP-Rh labelling of a band at ca. 100 kDa, which was annotated as DPP9 (98 kDa) in previous studies with FP-based ABPs.[22] Of note, DPP8 (103 kDa) would migrate in a similar region but has much lower expression levels, hampering its direct detection by this gel-based approach. Overall, the competitive gel ABPP approach suggested that *meta*-substituted *N*-phenyl 4-oxo-β-lactams, in contrast to *ortho*- or *para*-substituted analogues, might target DPP9 with high potency and significant selectivity, even in the presence of a full proteome.

A mass spectrometry-based ABPP approach using Stable Isotope Labeling with Amino acids in Cell culture (SILAC) quantification and the ABP **10** (Figure 3A), a biotin-labelled variant of **1**, in U937 cell lysates revealed several serine hydrolases as direct 4-oxo-β-lactam targets, including members of the DPP4 activity and/or structural homolog (DASH) family such as fibroblast activation

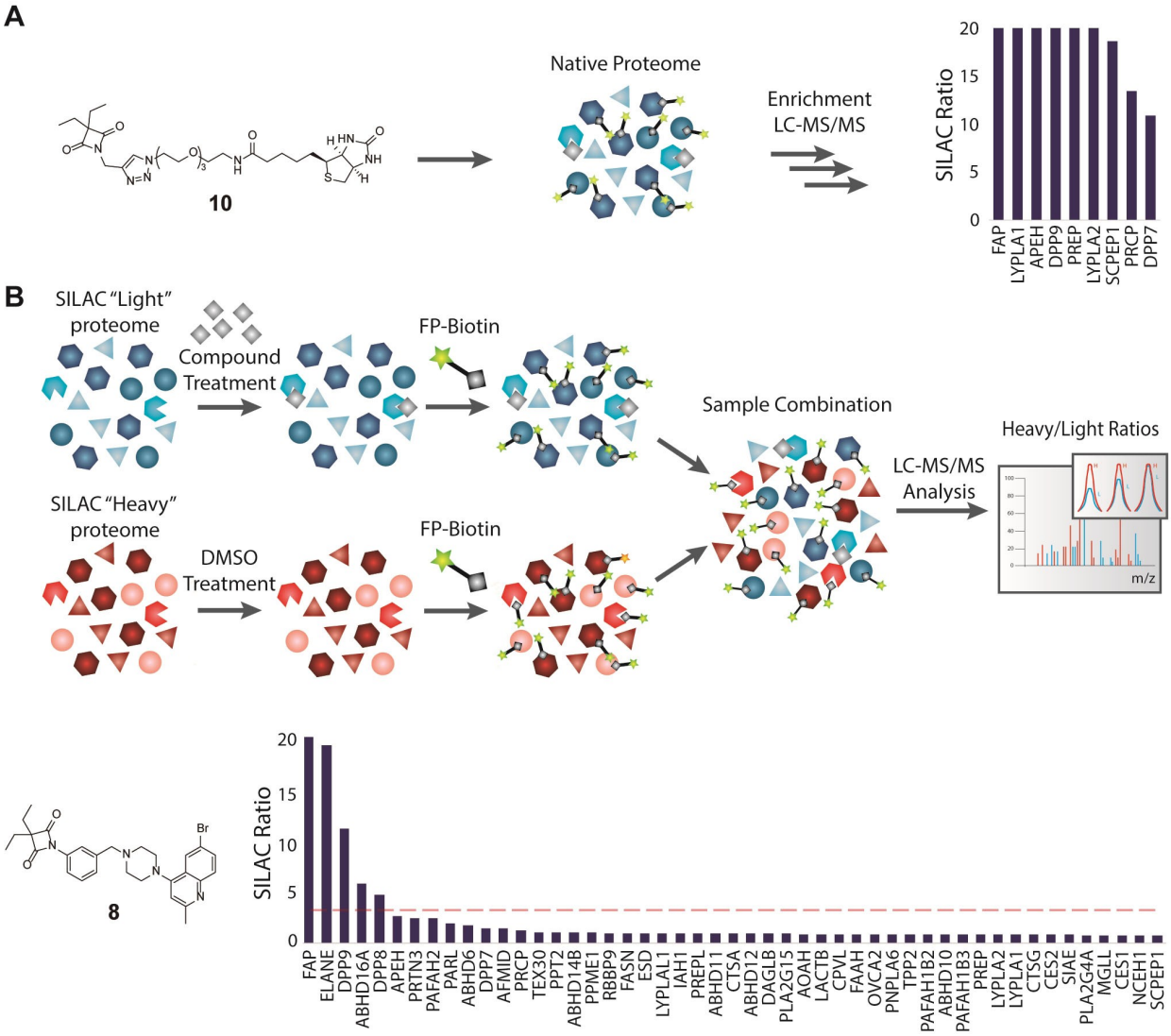

Figure 3. Identification of 4-oxo-β-lactam targets by mass-spectrometry based ABPP. A) Structure of the biotinylated 4-oxo-β-lactam ABP **10** and its use in a comparative ABPP approach. Enrichment of the direct targets of compound **10** (10 μM) (results filtered for SILAC Ratio > 3; Ratio = compound **10**/DMSO) confirmed labelling of several DPP enzymes, including DPP8 and DPP9. B) Overview on the competitive mass spectrometry-ABPP workflow (upper panel). (Lower panel) Competitive ABPP profiling with compound **8** (10 μM) and FP-biotin (10 μM) confirmed DPP8 and DPP9 as high occupancy targets of **8**, together with other enzymes like FAP and HNE (results filtered for serine hydrolases and SILAC Ratio > 3; Ratio = DMSO/compound **8**).

protein alpha (FAP), dipeptidyl peptidase 7 (DPP7), DPP9, as well as prolyl endopeptidase (PREP), acylaminoacyl-peptide hydrolase (APEH), lysophospholipase 1/2 (LYPLA1/2), serine carboxypeptidase 1 (SCPEP1) and prolyl carboxypeptidase (PRCP) (Figure 3A). In addition to the previously mentioned DPP-associated functions, these enzymes are related with important biological functions like lipid metabolism (LYPLA1 and 2), damaged protein turnover (APEH), hormone and neuropeptide metabolism (PREP) and blood pressure regulation (PRCP and SCPEP1), among other roles.[23] Importantly, all identified targets are proteins from the serine hydrolase family.

To validate the findings from the competitive gel-based ABPP experiments and to quantify target occupancy, we next used competitive mass spectrometry-based ABPP (Figure 3B) with the model compound **8**. To this end, SILAC U937 whole cell lysates were treated with either **8** or DMSO, followed by broadband serine hydrolase labelling with fluorophosphonate-biotin (FP-biotin). SILAC samples were combined, analysed by LC–MS/MS, and the resulting SILAC ratios were calculated, confirming the results from the competitive gel-based screen and revealing high target occupancy binding of **8** to only a small subset of serine hydrolases, including FAP, Human Neutrophil Elastase (ELANE), DPP9, ABHD16A and DPP8 (SILAC Ratio >3).

We were particularly intrigued that 4-oxo-β-lactams display a promising DPP8 and DPP9 inhibition profile and therefore decided to focus on investigating their molecular basis of inhibition and how this can be used to develop inhibitors with improved DPP8 vs. DPP9 inhibition selectivity. Our proteomics studies however showed that these compounds may also inhibit other enzymes such as FAP, ELANE or ABDH16A which has to be kept in mind when using these compounds in biological assays.

Given the novelty of the 4-oxo-β-lactam as a scaffold for DPP8/9 modulation, we wondered if our compounds shared structural similarity to previously reported DPP8/9 ligands. While some of our compounds contained recognition motifs known to efficiently contribute to DPP8/9 inhibition (e.g., the bisbenzyl system in **7** that is also found in 1G244), there was no previous report on the inhibition of these enzymes by a 4-oxo-β-lactam or other 4-membered ring chemotypes. We analysed the structural similarity of these compounds to known DPP8/9 inhibitors described in ChEMBL v27 by t-distributed stochastic neighborhood embedding (t-SNE). Using the ECFP4-like Morgan fingerprint (radius 2, 2048 bits), we obtained an average Tanimoto index <0.13 when comparing **6–9** to DPP8/9 reference ligands. In all cases, a Tanimoto similarity lower than 0.34 was found for their nearest neighbours which is well below the usual threshold of 0.85 that denotes similar ligands (a Tanimoto index of 1.0 denotes two identical molecules while a value of 0 denotes complete dissimilarity).[24] This data further corroborates 4-oxo-β-lactams as a novel chemotype in the DPP8/9 inhibitor space as a result from an unusual topological pharmacophore feature arrangement, and is exemplified by their outlier position in the DPP8/9 inhibitor cluster (Supporting Information Figure S1.4.).

Concentration-dependent competitive labelling experiments with **6–8** and the ABP FP-Rh in cells overexpressing selected DASH family hydrolases allowed determination of their inhibitory IC_{50} values in a complex proteome (Table 1). The compounds potently inhibited DPP8 and DPP9 in the nanomolar range (**8** inhibited DPP9 in low micromolar range), with **6** being moderately more active. In all cases, DPP8 was more potently inhibited than DPP9 (IC_{50} of 137 nM vs. 409 nM for **6**, 393 nM vs. 950 nM for **7**, 292 nM vs. 1033 nM for **8**). DPP4 was approximately 10-times less efficiently inhibited and DPP7 was not inhibited at all at the tested concentration range. Overall, these ABPP experiments indicate that **6–8** potently inhibit DPP8 and DPP9 as high target occupancy labelling events.

While competitive ABPP screening is invaluable in providing early access to potency and selectivity properties of chemical inhibitors in complex proteomes, a systematic determination of structural determinants relevant for inhibition can be hindered by various factors such as problems arising from different enzyme expression levels of DPP8 and DPP9 in cells.

To gain further insight into the structural determinants underlying DPP8 or DPP9 inhibition, selected 4-oxo-β-lactam derivatives were synthesized and tested in biochemical inhibition assays; the corresponding results are reported in Table 2 and Supporting Table S1.5. Along these lines, we first determined the *Ki′* of **6** in these assay conditions and confirmed potent, nanomolar inhibition of DPP8 (26.3 nM) and a ca. 7-fold less potent, nevertheless still nanomolar inhibition of DPP9 (184 nM). We then investigated the impact of a structural reduction of the inhibitor by removal of the terminal aryl moiety (compound **11**, Table 2). **11** displayed a *Ki′* of 528 nM for DPP8 and was inactive towards DPP9 in the tested concentration range. Interestingly, further structural reduction by additional removal of the piperazine moiety then led to a completely inactive compound at the tested concentrations (Supporting Information Table S1.5.).

To shed light on the underlying molecular basis of inhibition, we performed X-ray structural analyses of **6** and **11** in complex with DPP8. The obtained structures contained two protomers in their asymmetric unit and a final resolution of 2.6 and 2.8 Å for **6** and **11**, respectively. Electron densities unambiguously demonstrated the presence of a covalent bond between the different ligands and DPP8 through acylation of the S755 residue. Interestingly, binding of **6** to DPP8 occurred via an unprecedented binding mode (Figure 4A): instead of occupying the S2–S1 subsites which are accommodated by substrate-derived inhibitors

Table 1: IC_{50} values [nM] determined by competitive ABPP for the 4-oxo-β-lactams **6–8**.

	6	**7**	**8**
DPP8	137 ± 40	393 ± 55	292 ± 42
DPP9	409 ± 78	950 ± 297	1033 ± 225
DPP4	1398 ± 298	1182 ± 444	2699 ± 617
DPP7	>10000	>10000	>10000

Table 2: Inhibition profile of 4-Oxo-β-Lactams.

	R	*Ki′* [nM][a] DPP8	DPP9	DPP8/DPP9 Selectivity
6	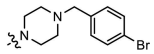	26.3 ± 2.6	184 ± 38.4	7×
11		528 ± 175.5	> 2000	> 4×
12	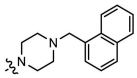	95.0 ± 15.5	> 2000	> 21×
13	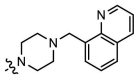	174 ± 55.3	34.2 ± 30	0.2×
14	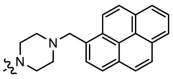	> 2000	> 2000	n.a.
9	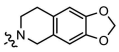	2.7 ± 0.6	11.4 ± 3.5	4×

[a] apparent *Ki* values (*Ki′*) were calculated from enzyme kinetic analyses in presence of different inhibitor concentrations and fitting with the Morrison equation. This equation is usually used for tight-binding inhibition and represents a suitable proxy for covalent inhibition. Errors represent the 95% confidence interval fit.

such as VbP or 1G244, the terminal aryl moiety of **6** protrudes into a previously unrecognized non-substrate like hydrophobic subsite located in vicinity of the S2′ subsite (we will refer to this region as an extended S2′ (eS2′) subsite from here on). Additionally, no ordering transition of the R-segment occurred and a highly disordered H865 segment (Figure 4A, indicated with an arrow) as well as a disrupted SUBA-domain (SUMO-binding arm for activation of DPP8/9) was observed.[25] The importance of the terminal aryl moiety for accomplishing this binding mode was demonstrated by the cocrystal structure with **11** (Figure 4B): absence of this moiety resulted in an overall turn of the binding orientation into the S2–S1 subsites, an induction of a partially ordered R-segment and the presence of a structured H865 segment and the SUBA-domain. An ordered H865 segment is required for substrate binding and plays a key role in ordering of the catalytic triad (S755-H865-D833). These results thus indicate that **6** seems to induce a catalytically incompetent conformation while **11** binds in a classical substrate-like fashion. This finding shows that the 4-oxo-β-lactams can adopt two different binding modes, substrate- vs. non-substrate-like. The selection for the non-substrate-like binding mode is thereby triggered by proper derivatization at the piperazine moiety.

To explore the impact of the aryl handle on inhibition, derivatives with a naphthalene or quinoline residue instead of the bromophenyl residue were also generated (Table 2, compounds **12**–**13**). From all synthesized compounds (Table 2 and Supporting Information Table S1.5.), the naphthalene compound **12** was the most selective DPP8 inhibitor, inhibiting DPP8 with a $Ki' = 95.0$ nM, while DPP9 was not inhibited at the tested concentrations ($Ki' >$ 2000 nM, resulting in a at least 21-fold selectivity). The crystal structure of **12**:DPP8 showed a similar ligand-protein interaction pattern as **6** (Figure 5A), highlighting again the relevance of the eS2′ site for DPP8 inhibition. In contrast, the quinoline compound **13** that differs from **12** only by the presence of a nitrogen moiety in the aromatic system, was a better DPP9 than DPP8 inhibitor (DPP9 $Ki' = 34.2$ nM vs. DPP8 $Ki' = 174$ nM, 5-fold DPP9 selective). To investigate the molecular basis of its potent binding to DPP9, an X-ray structure of **13** in complex with DPP9 was measured. This analysis revealed that **13**, in contrast to the binding mode observed in **12**:DPP8, binds in a classical substrate-like manner, i.e., it occupies the S2–S1 subsites of DPP9 (Figure 5B), despite the apparent presence of an eS2′ subsite

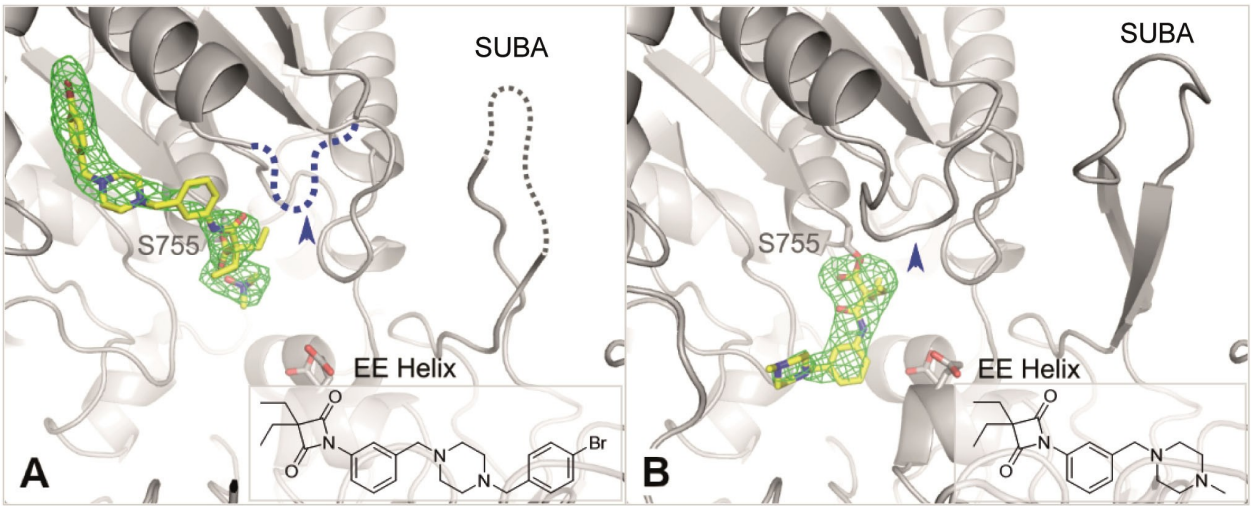

Figure 4. X-ray analyses of **6** (PDB ID: 7OZ7) and **11** (PDB ID: 7A3L) in complex with DPP8 revealed two distinct binding modes. The omit map difference electron density ($F_o - F_c$) for the ligands is displayed at 3σ. A) **6** occupies the S1′ and an eS2′ subsite. Binding is associated with a disordering of the H865 segment (blue arrow) and of the SUBA domain. B) In contrast, **11** binds to the S2–S1 subsites frequently occupied by classical mechanism based DPP8 inhibitors. The corresponding H865 (blue arrow) and SUBA domains remain ordered.

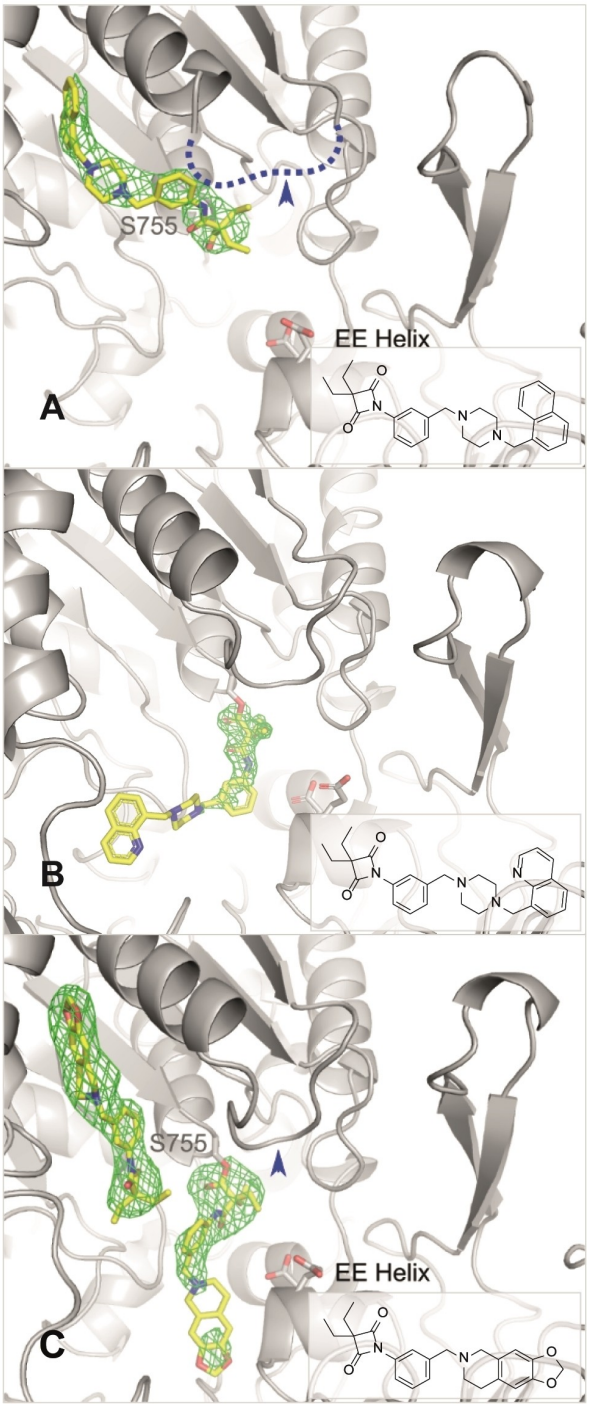

Figure 5. X-ray analysis of **12** (PDB ID: 7A3J) and **9** (PDB ID: 7A3G) in complex with DPP8 and **13** (PDB ID: 7ZXS) in complex with DPP9 reveals three distinct binding modes. The omit map difference electron density (F_o-F_c) for the ligands is displayed at 3σ. A) **12** displays the best DPP8 selectivity. Its overall binding mode resembles the one observed for **6**, indicating that subtle interactions at the end of the pocket define DPP8 vs. DPP9 selectivity. B) The **13**:DPP9 structure shows the classical substrate-like inhibitor alignment, occupying the S2–S1 subsites. C) **9** is the most potent DPP8 and DPP9 inhibitor of the compound series. Its binding mode is more complex, consisting of an arrangement of two ligands into the active site region; one ligand binds to the S2–S1 subsites, while the second occupies the S1′–eS2′ subsite region.

also in DPP9. We can therefore only speculate why eS2′ is not targeted by **13**. One such explanation could be a slight shift of the orientation of arginine residue R843 (R868 in DPP8) which could partially occlude entry into this subsite. Independently of the exact mechanism underlying the selection of the binding mode, these findings indicate that inhibitors targeting eS2′ in DPP8 may display potential DPP8 vs. DPP9 selectivity. The eS2′ subsite thereby seems to display defined structural determinants as introduction of a spatially more demanding pyrene substituent (compound **14**) instead of the naphthalene residue led to an inactive compound, indicating a limited steric tolerance. The introduction of a flatter and conformationally less flexible TDIQ substituent in **9** resulted in the most potent inhibitor of this study ($Ki'=2.7$ nM for DPP8 and 11.4 nM for DPP9). Yet, DPP8 vs. DPP9 selectivity was weak and crystallographic analysis of the binding mode revealed a complex binding pattern, consisting of the simultaneous alignment of two ligand molecules in the binding pocket (Figure 5C). Indeed, one ligand was covalently bound to the S755 residue and pointed in a substrate-like fashion towards the EE helix; the other ligand occupied the eS2′ subsite via a non-covalent interaction. This "dual binding mode" together with the previous findings suggest that both binding to the S2–S1 subsites or to the hydrophobic DPP8 pocket results in similar binding affinities. On the other hand, selectivity seems to be driven by preferential binding to the S1′–eS2′ subsites.

Overall, we propose that the differential binding mode and specificity of these ligands depend upon divergent structural features of DPP8 and DPP9. Specifically, an extended active site on DPP8 can more easily exhibit the two ligand binding configurations observed in our study, with inhibitors targeting the eS2′ subsite causing high structural instability on DPP8. Conversely, DPP9 has a more strict ligand binding mode, limiting the orientation of molecules to only substrate-like types. Moreover, DPP9 does not show signs of structural instability, and in contrast to the DPP8-ligand-bound structures, the R-helix and additional structural motives are clearly defined by electron density. Of note, these findings were corroborated by the synthesis and structural analysis of further 4-oxo-β-lactam derivatives; for these cases, more selective inhibitors preferred accommodation of the S1′–eS2′ subsites in DPP8 (Supporting Information Table S1.5. and Supporting Information Figure S1.6.).

So far, the developed 4-oxo-β-lactams were shown to display promising DPP8/9 inhibitory properties in biochemical assays. DPP8/9 inhibitors like VbP and 1G244 are known to promote activation of the NLRP1 inflammasome, with maturation of pro-inflammatory cytokines such as IL-1β or IL-18, followed by a specific form of lytic cell death called pyroptosis.[4d,e,13] To demonstrate target engagement of 4-oxo-β-lactams also in living cells, we therefore determined compound-triggered inflammasome activation in myeloid cells. To this end, we quantified IL-1β and lactate dehydrogenase (LDH) as a measure of lytic cell death in murine bone marrow-derived dendritic cells (BMDCs) after treatment with the 4-oxo-β-lactams **6**, **9** and **12** or the

positive controls VbP and 1G244 (Figure 6A). All three 4-oxo-β-lactams triggered caspase-1 dependent IL-1β release, as well as pyroptosis in a concentration dependent manner, with **9** being most active. All three compounds were, however, less active than the control compounds VbP or 1G244.

In contrast to humans, mice carry several NLRP1 paralogs, one of which, NLRP1b, is missing in C57bl/6 mice. Consistent with the activation of multiple NLRP1 paralogs by DPP8/9 inhibitors, treatment of cells derived from Balb/c mice with the 4-oxo-β-lactams **6**, **9** and **12** as well as the control compound 1G244 led to a much stronger inflammasome response than the analogous treatment of cells from C57bl/6 mice (Figure 6B). In cells from Balb/c mice, the 4-oxo-β-lactams **6** and **9** were more active than **12**. In agreement with a NLRP3-mediated inflammasome activation, nigericin treatment was equally potent in cells from either mouse line. Cleavage of the inflammasome effector protease caspase-1 and its pore-forming substrate gasdermin D as additional hallmarks of inflammasome activation was confirmed by western blot (Supporting Information Figure S1.7.). Importantly, the potential off-targets identified in MS-based assays are not associated with DPP8/9's effects in inflammasome activation and pyroptosis and should not interfere with these assays. FAP is involved in cell death and ABHD16A is associated with lyso-PS and lipopolysaccharide-induced cytokine production,[23,26] but both seem to have no direct relation with inflammasome activation. ELANE has recently been associated with neutrophil-specific pathways downstream to inflammasome activation, but while this pathway can be associated with IL-1β release, it is a pyroptosis-independent, non-lytic pathway, which results in no increase in LDH release.[27] Together, these findings demonstrate inflammasome activation and thus DPP8/9 target engagement in primary immune cells.

Conclusion

The pursuit of selective inhibitors of DPP8 and DPP9 is a current hot topic in chemical biology and an ongoing drug design challenge intimately associated with the high structural similarity and shared substrate specificity of these enzymes. Here, using an integrated and non-directed gel- and mass spectrometry-based ABPP platform, we uncovered the hidden pharmacology of 4-oxo-β-lactams and found that *meta*-substituted *N*-aryl 4-oxo-β-lactams are potent and structurally diverse DPP8 and DPP9 inhibitors with high target occupancy and promising potency and selectivity. By combining proteomics, chemical synthesis, structural biology, and bioinformatics analyses, we were able to prototype 4-oxo-β-lactams as an innovative chemotype for DPP8 modulation, with rationally designed 4-oxo-β-lactam inhibitors achieving unprecedented levels of DPP8/9 selectivity, e.g., reflected by compound **12** (>21× selective towards DPP8) or compound **13** (>5× selective towards DPP9). Elucidation of the ligand-protein crystal structures of 4-oxo-β-lactams with either DPP8 or DPP9 then revealed the presence of a previously unrecognized eS2′ subsite in DPP8 whose targeting by inhibitors may confer DPP8 vs. DPP9 selectivity.

Our studies thus suggest that a rational modification of "classical" substrate-like inhibitors with structural units targeting the here elucidated eS2′ subsite may hold the key to more potent and selective DPP8 inhibitors. This valuable structural data, which was absent in past DPP8/9 studies,

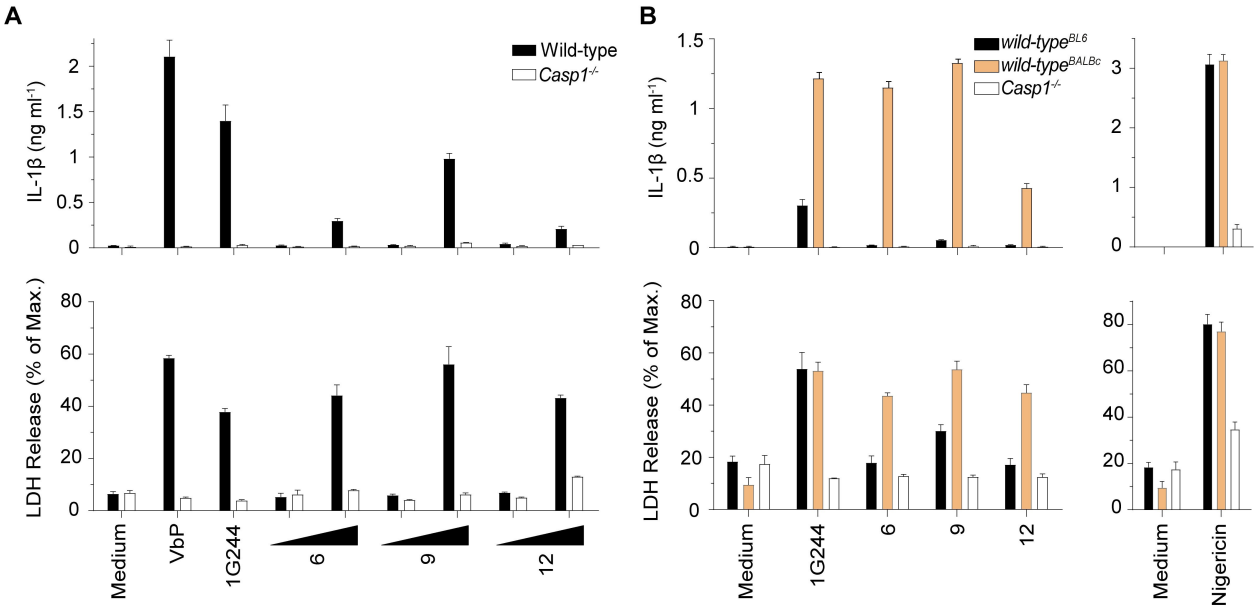

Figure 6. Inflammasome activation by DPP8/9 inhibitors. A) Wild-type and Caspase 1-deficient BMDCs were primed with LPS and then stimulated with 5 μM nigericin, 10 μM VbP, 10 μM 1G244 or increasing concentrations of **6**, **9** and **12** (10 and 100 μM) for 16 hr. B) Wild-type C57bl/6, Balb/c and Caspase 1-deficient BMDCs were primed with LPS and then stimulated with 5 μM nigericin, 10 μM VbP, 10 μM 1G244 or 100 μM of **6**, **9** and **12** for 16 hr. Releases of IL-1β and LDH into the supernatants were measured by an ELISA and a colorimetric assay, respectively.

helped us to develop inhibitors with the highest DPP8/9 selectivity index described to date and will be crucial in supporting future inhibitor design.

Importantly, while the ABPP experiments suggest a good degree of selectivity within the serine hydrolase family, caution and suitable controls should nevertheless be taken when using these inhibitors in biological assays probing DPP8/9 function as we cannot completely rule out other off-target effects of our compounds.

Overall, the powerful and integrated platform combining ABPP techniques and classical drug design unlocks access to early data on potency and selectivity of compound leads and is invaluable in avoiding pitfalls later in the drug development pipeline.

Acknowledgements

This study was supported by Fundação para a Ciência e a Tecnologia (FCT, Portugal) through projects PTDC/MED-CAR/31322/2017, SAICTPAC/0019/2015, PTDC/MED-QUI/30021/2017, UIDB/04138/2020 and UIDP/04138/2020, fellowship SFRH/BD/100400/2014 (L.A.R.C.), SFRH/BD/137459/2018 (R. F.) and by European Union's Structural & Investment Funds through COMPETE—POCI, under programme grant LISBOA-01-0145-FEDER-016405. L.A.R.C. was sponsored by an FCT-funded Fulbright Grant. R.G.-F. acknowledges funding from the Deutsche Forschungsgemeinschaft (DFG) Grant 2234/1-3 and the DFG GRK2606 (Project ID 423813989). B.R. held a fellowship of the Peter and Traudl Engelhorn Stiftung. Work in the laboratory of O.G. is supported by the Deutsche Forschungsgemeinschaft (DFG, German Research Foundation) through SFB 1160 (Project ID 256073931), SFB/TRR 167 (Project ID 259373024), SFB 1425 (Project ID 422681845), SFB 1479 (Project ID 441891347), GRK 2606 (Project ID 423813989) and under the Germany's Excellence Strategy (CIBSS—EXC-2189—Project ID 390939984), as well as by the European Research Council (ERC) through Proof-of-Concept Grant 966687 and Marie Skłodowska-Curie Grant 101034170 (Cofund: EURIdoc). M.K. acknowledges support by the Deutsche Forschungsgemeinschaft (SFB1430). B.C. acknowledges support of NIH R35 CA231991. The authors thank Ulrike Möller for technical assistance.

Conflict of Interest

The authors declare no conflict of interest.

Data Availability Statement

The data that support the findings of this study are available in the Supporting Information of this article.

Keywords: Activity-Based Protein Profiling · Dipeptidyl Peptidases 8/9 · 4-Oxo-β-Lactams · Proteomics · X-Ray Diffraction

[1] H. Zhang, Y. Chen, F. M. Keane, M. D. Gorrell, *Mol. Cancer Res.* **2013**, *11*, 1487–1496.

[2] a) C. A. Abbott, D. M. T. Yu, E. Woollatt, G. R. Sutherland, G. W. McCaughan, M. D. Gorrell, *Eur. J. Biochem.* **2000**, *267*, 6140–6150; b) C. Olsen, N. Wagtmann, *Gene* **2002**, *299*, 185–193; c) B. Ahrén, *Front. Endocrinol.* **2019**, *10*, 376.

[3] M. C. Okondo, D. C. Johnson, R. Sridharan, E. B. Go, A. J. Chui, M. S. Wang, S. E. Poplawski, W. Wu, Y. Liu, J. H. Lai, D. G. Sanford, M. O. Arciprete, T. R. Golub, W. W. Bachovchin, D. A. Bachovchin, *Nat. Chem. Biol.* **2017**, *13*, 46–53.

[4] a) D. C. Johnson, C. Y. Taabazuing, M. C. Okondo, A. J. Chui, S. D. Rao, F. C. Brown, C. Reed, E. Peguero, E. de Stanchina, A. Kentsis, D. A. Bachovchin, *Nat. Med.* **2018**, *24*, 1151–1156; b) M. C. Okondo, S. D. Rao, C. Y. Taabazuing, A. J. Chui, S. E. Poplawski, D. C. Johnson, D. A. Bachovchin, *Cell Chem. Biol.* **2018**, *25*, 262–267; c) N. M. de Vasconcelos, G. Vliegen, A. Gonçalves, E. De Hert, R. Martín-Pérez, N. Van Opdenbosch, A. Jallapally, R. Geiss-Friedlander, A.-M. Lambeir, K. Augustyns, P. Van der Veken, I. De Meester, M. Lamkanfi, *Life Sci. Alliance* **2019**, *2*, e201900313; d) K. Gai, M. C. Okondo, S. D. Rao, A. J. Chui, D. P. Ball, D. C. Johnson, D. A. Bachovchin, *Cell Death Dis.* **2019**, *10*, 587; e) L. R. Hollingsworth, H. Sharif, A. R. Griswold, P. Fontana, J. Mintseris, K. B. Dagbay, J. A. Paulo, S. P. Gygi, D. A. Bachovchin, H. Wu, *Nature* **2021**, *592*, 778–783; f) C. Lu, J. U. Tilan, L. Everhart, M. Czarnecka, S. J. Soldin, D. R. Mendu, D. Jeha, J. Hanafy, C. K. Lee, J. Sun, E. Izycka-Swieszewska, J. A. Toretsky, J. Kitlinska, *J. Biol. Chem.* **2011**, *286*, 27494–27505; g) R. Han, X. Wang, W. Bachovchin, Z. Zukowska, J. W. Osborn, *Sci. Rep.* **2015**, *5*, 12348; h) V. Dubois, C. V. Ginneken, H. D. Cock, A.-M. Lambeir, P. Van der Veken, K. Augustyns, X. Chen, S. Scharpé, I. D. Meester, *J. Histochem. Cytochem.* **2009**, *57*, 531–541; i) P. A. Spagnuolo, R. Hurren, M. Gronda, N. MacLean, A. Datti, A. Basheer, F. H. Lin, X. Wang, J. Wrana, A. D. Schimmer, *Leukemia* **2013**, *27*, 1236–1244; j) K. P. Moore, A. G. Schwaid, M. Tudor, S. Park, D. C. Beshore, A. Converso, W. D. Shipe, R. Anand, P. Lan, R. Moningka, D. M. Rothman, W. Sun, A. Chi, I. Cornella-Taracido, G. C. Adam, C. Bahnck-Teets, S. S. Carroll, J. F. Fay, S. L. Goh, J. Lusen, S. Quan, S. Rodriguez, M. Xu, C. L. Andrews, C. Song, T. Filzen, J. Li, K. Hollenstein, D. J. Klein, A. Lammens, U. M. Lim, Z. Fang, C. McHale, Y. Li, M. Lu, T. L. Diamond, B. J. Howell, P. Zuck, C. J. Balibar, *ACS Chem. Biol.* **2022**, *17*, 2595–2604.

[5] a) T. Sato, A. Tatekoshi, K. Takada, S. Iyama, Y. Kamihara, P. Jawaid, M. U. Rehman, K. Noguchi, T. Kondo, S. Kajikawa, K. Arita, A. Wada, J. Murakami, M. Arai, I. Yasuda, N. H. Dang, R. Hatano, N. Iwao, K. Ohnuma, C. Morimoto, *Sci. Rep.* **2019**, *9*, 18094; b) Z. Tang, J. Li, Q. Shen, J. Feng, H. Liu, W. Wang, L. Xu, G. Shi, X. Ye, M. Ge, X. Zhou, S. Ni, *Int. J. Cancer* **2017**, *140*, 1620–1632.

[6] a) R. Geiss-Friedlander, N. Parmentier, U. Moller, H. Urlaub, B. J. Van den Eynde, F. Melchior, *J. Biol. Chem.* **2009**, *284*, 27211–27219; b) D. Justa-Schuch, M. Silva-Garcia, E. Pilla, M. Engelke, M. Kilisch, C. Lenz, U. Möller, F. Nakamura, H. Urlaub, R. Geiss-Friedlander, *eLife* **2016**, *5*, e16370; c) O. Bolgi, M. Silva-Garcia, B. Ross, E. Pilla, V. Kari, M. Killisch, M. Spitzner, N. Stark, C. Lenz, K. Weiss, L. Donzelli, M. D. Gorrell, M. Grade, J. Riemer, H. Urlaub, M. Dobbelstein, R. Huber, R. Geiss-Friedlander, *EMBO Rep.* **2022**, e54136.

[7] M. Sharif-zak, M. Abbasi-jorjandi, G. Asadikaram, Z. A. Ghoreshi, M. Rezazadeh-Jabalbarzi, A. Afsharipur, H. Rashi-

dinejad, F. Khajepour, A. Jafarzadeh, N. Arefinia, A. Kheyrkhah, M. Abolhassani, *Immunobiology* **2022**, *227*, 152184.
[8] a) J. R. Bjelke, J. Christensen, P. F. Nielsen, S. Branner, A. B. Kanstrup, N. Wagtmann, H. B. Rasmussen, *Biochem. J.* **2006**, *396*, 391–399; b) B. Ross, S. Krapp, M. Augustin, R. Kierfersauer, M. Arciniega, R. Geiss-Friedlander, R. Huber, *Proc. Natl. Acad. Sci. USA* **2018**, *115*, 1437–1445.
[9] L. Heirbaut, S. van Goethem, K. Jansen, H. de Winter, N. Lamoen, J. Joossens, J. Cheng, X. Chen, A.-M. Lambeir, I. de Meester, K. Augustyns, P. Van der Veken, *MedChemComm* **2016**, *7*, 433–438.
[10] a) W.-T. Jiaang, Y.-S. Chen, T. Hsu, S.-H. Wu, C.-H. Chien, C.-N. Chang, S.-P. Chang, S.-J. Lee, X. Chen, *Bioorg. Med. Chem. Lett.* **2005**, *15*, 687–691; b) J.-J. Wu, H.-K. Tang, T.-K. Yeh, C.-M. Chen, H.-S. Shy, Y.-R. Chu, C.-H. Chien, T.-Y. Tsai, Y.-C. Huang, Y.-L. Huang, C.-H. Huang, H.-Y. Tseng, W.-T. Jiaang, Y.-S. Chao, X. Chen, *Biochem. Pharmacol.* **2009**, *78*, 203–210.
[11] S. van Goethem, V. Matheeussen, J. Joossens, A.-M. Lambeir, X. Chen, I. De Meester, A. Haemers, K. Augustyns, P. Van der Veken, *J. Med. Chem.* **2011**, *54*, 5737–5746.
[12] E. Pilla, M. Kilisch, C. Lenz, H. Urlaub, R. Geiss-Friedlander, *J. Biol. Chem.* **2013**, *288*, 32787–32796.
[13] T. A. Kelly, J. Adams, W. W. Bachovchin, R. W. Barton, S. J. Campbell, S. J. Coutts, C. A. Kennedy, R. J. Snow, *J. Am. Chem. Soc.* **1993**, *115*, 12637–12638.
[14] P. Van der Veken, A. Soroka, I. Brandt, Y.-S. Chen, M.-B. Maes, A.-M. Lambeir, X. Chen, A. Haemers, S. Scharpé, K. Augustyns, I. De Meester, *J. Med. Chem.* **2007**, *50*, 5568–5570.
[15] B. Ross, S. Krapp, R. Geiss-Friedlander, R. Huber, *Acta Crystallogr. Sect. A* **2018**, *74*, e228.
[16] M. J. Niphakis, B. F. Cravatt, *Annu. Rev. Biochem.* **2014**, *83*, 341–377.
[17] B. F. Cravatt, A. T. Wright, J. W. Kozarich, *Annu. Rev. Biochem.* **2008**, *77*, 383–414.
[18] a) W. P. Heal, T. H. T. Dang, E. W. Tate, *Chem. Soc. Rev.* **2011**, *40*, 246–257; b) D. Leung, C. Hardouin, D. L. Boger, B. F. Cravatt, *Nat. Biotechnol.* **2003**, *21*, 687–691.
[19] J. Mulchande, R. C. Guedes, W.-Y. Tsang, M. I. Page, R. Moreira, J. Iley, *J. Med. Chem.* **2008**, *51*, 1783–1790.
[20] E. F. Ruivo, L. M. Goncalves, L. A. Carvalho, R. C. Guedes, S. Hofbauer, J. A. Brito, M. Archer, R. Moreira, S. D. Lucas, *ChemMedChem* **2016**, *11*, 2037–2042.
[21] Y. Liu, M. P. Patricelli, B. F. Cravatt, *Proc. Natl. Acad. Sci. USA* **1999**, *96*, 14694–14699.
[22] D. A. Bachovchin, T. Ji, W. Li, G. M. Simon, J. L. Blankman, A. Adibekian, H. Hoover, S. Niessen, B. F. Cravatt, *Proc. Natl. Acad. Sci. USA* **2010**, *107*, 20941–20946.
[23] J. Z. Long, B. F. Cravatt, *Chem. Rev.* **2011**, *111*, 6022–6063.
[24] J. J. Irwin, D. Duan, H. Torosyan, A. K. Doak, K. T. Ziebart, T. Sterling, G. Tumanian, B. K. Shoichet, *J. Med. Chem.* **2015**, *58*, 7076–7087.
[25] E. Pilla, U. Möller, G. Sauer, F. Mattiroli, F. Melchior, R. Geiss-Friedlander, *J. Biol. Chem.* **2012**, *287*, 44320–44329.
[26] S. S. Kamat, K. Camara, W. H. Parsons, D. H. Chen, M. M. Dix, T. D. Bird, A. R. Howell, B. F. Cravatt, *Nat. Chem. Biol.* **2015**, *11*, 164–171.
[27] M. Karmakar, M. Minns, E. N. Greenberg, J. Diaz-Aponte, K. Pestonjamasp, J. L. Johnson, J. K. Rathkey, D. W. Abbott, K. Wang, F. Shao, S. D. Catz, G. R. Dubyak, E. Pearlman, *Nat. Commun.* **2020**, *11*, 2212.

Manuscript received: July 18, 2022
Accepted manuscript online: September 11, 2022
Version of record online: October 28, 2022